1. X-Ray Powder Diffraction data analysis

The X-ray powder diffraction (XRPD) pattern was recorded with a *Bruker D8 Advance* diffractometer configured in Debye-Scherrer geometry. Crystal structure determination was performed with the *MS Reflex Plus* module within the *Accelrys Materials Studio*® suite. The Parallel Tempering algorithm was employed for structure solution search by refining 24 structural degrees of freedom (DOF), out of which 13 are flexible torsion angles in the Lisinopril molecule. Two types of searches over the so defined DOF space were performed: *complete*, which uses the maximum number of steps/run corresponding to the number of the DOF and the employed parameters of the Parallel Tempering algorithm, and *restricted*, with about 50 times less steps/run. Taking R_{wp} fit factors obtained in the first case as a reference, it was concluded that 15 runs were sufficient to achieve good convergence under *restricted* search – see the data listed in Tab. E1. Three crystal structure solutions with R_{wp} < 5 %, *LisiRef*, *Lisi1*, and *Lisi2* (marked in bold, and taken in the order they occur in Tab. E1), are selected for further analysis, because they span the full variation range with respect to the type of search and carboxyls conformation. The most relevant parameters of these models are given in Tab. E2. Representative crystallographic data for the structure model determined with the lowest figure of merit (*Lisi1*: R_{wp} = 4.6 %) are presented in Fig. E1. The long range ordering and major crystal packing patterns identified in Lisinopril dihydrate are shown in Fig. E2. For the all models, the hydrogen bonding networks that form depending on the particular conformation of the C10-OOH / C21-OOH carboxyl, and N2-H amine are emphasized in Figs. E3-E4: corresponding geometric parameters are listed in Tables E3-E4.

Table E1: Representative parameters for structure solution search. For each solution, there are listed: R_{wp} figures of merit before and after Rietveld refinement; particular conformations of the specified carboxyl groups: s - close to the *syn*, and a - close to the *anti*, conformation of the N2-C9-C10-O1 and N3-C17-C21-O4 moieties, with variations of the corresponding torsion angle of ±25^0 around perfect planarity

Type of search	No. of runs	Steps / run	search time	R_{wp} [%] structure solution	R_{wp} [%] Rietveld refinement	C10-OOH conformation	C21-OOH conformation
complete	3	2.15×10^9	~ 6 days	6.7; **6.1**; 7.2	5.1; **4.8**; 5.3	s; **a**; a	a; **s**; a
restricted	15	4×10^7	~ 10 hours	10.1; 7.5; 12.6; 11.6; 12.7; **6.5**; 12.3; 10.6; 12.8; **6.4**; 11.8; 12.4; 12.0; 10.1; 6.4	7.4; 5.3; 9.9; 8.1; 7.9; **4.6**; 8.2; 6.8; 7.3; **4.9**; 7.5; 8.9; 11.3; 9.1; 4.8	s; a; s; s; s; **s**; s; s; a; **a**; s; s; s; a; s	s; a; a; s; s; **s**; a; s; s; **a**; s; a; s; s; s

Table E2: Comparative analysis of the *LisiRef*$^{(0)}$, *Lisi1*$^{(0)}$, and *Lisi2*$^{(0)}$, i.e., the Rietveld refined crystal structure models with DFT geometry optimization of only the hydrogen positions, in terms of: R_{wp} figure of merit; RMSD of the Lisinopril molecular structure relative to the molecule in the *Lisi1*$^{(0)}$ model obtained with the lowest R_{wp} (only the heavy atoms are considered, and no distinction between single and double bonded oxygen atoms in the carboxyl groups is made); C10-OOH / C21-OOH carboxyl groups conformations; energy variation ΔE relative to the lowest energy XRPD structure (*LisiRef*$^{(0)}$); O-O distances and O-O-O angles between consecutive oxygen atoms in the *A* and *B* water chains.

Model	R_{wp} [%]	Lisinopril RMSD [Å]	Carboxyls conformations C10-OOH / C21-OOH	ΔE [kcal/mol]	O-O [Å] / O-O-O [^{0}]	
					water chain *A*	water chain *B*
LisiRef$^{(0)}$	4.84	0.018	a / s	0	3.18 / 136	3.42 / 119
Lisi1$^{(0)}$	4.60	0	s / s	13.6	3.24 / 131	3.43 / 119
Lisi2$^{(0)}$	4.91	0.027	a / a	12.2	3.18 / 136	3.33 / 125

Chemical Formula	$C_{21}H_{31}N_3O_5 \cdot 2H_2O$
M_r	447
Crystal system	Monoclinic
Space group	*P21*
a (Å)	14.6450(6)
b (Å)	5.906(2)
c (Å)	14.299(4)
β	113.1(1)
V (Å^3)	1137.76
Z	6
D_{calc} (g/cm^3)	1.29
Data range	$3.992^o \leq 2\theta \leq 44.986^o$
Step size	0.008º
λ (Å)	1.54065
T	295 K
R_{wp}	4.60 %
R_p	3.47 %

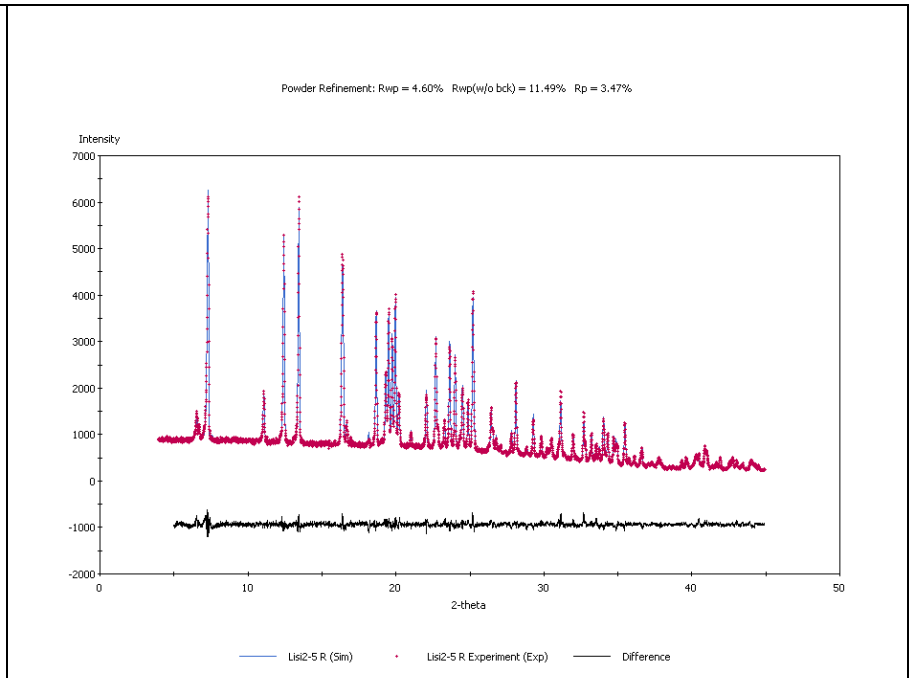

Fig. E1 *Crystallographic data and the Rietveld refinement plot for Lisinopril dihydrate, model* Lisi1

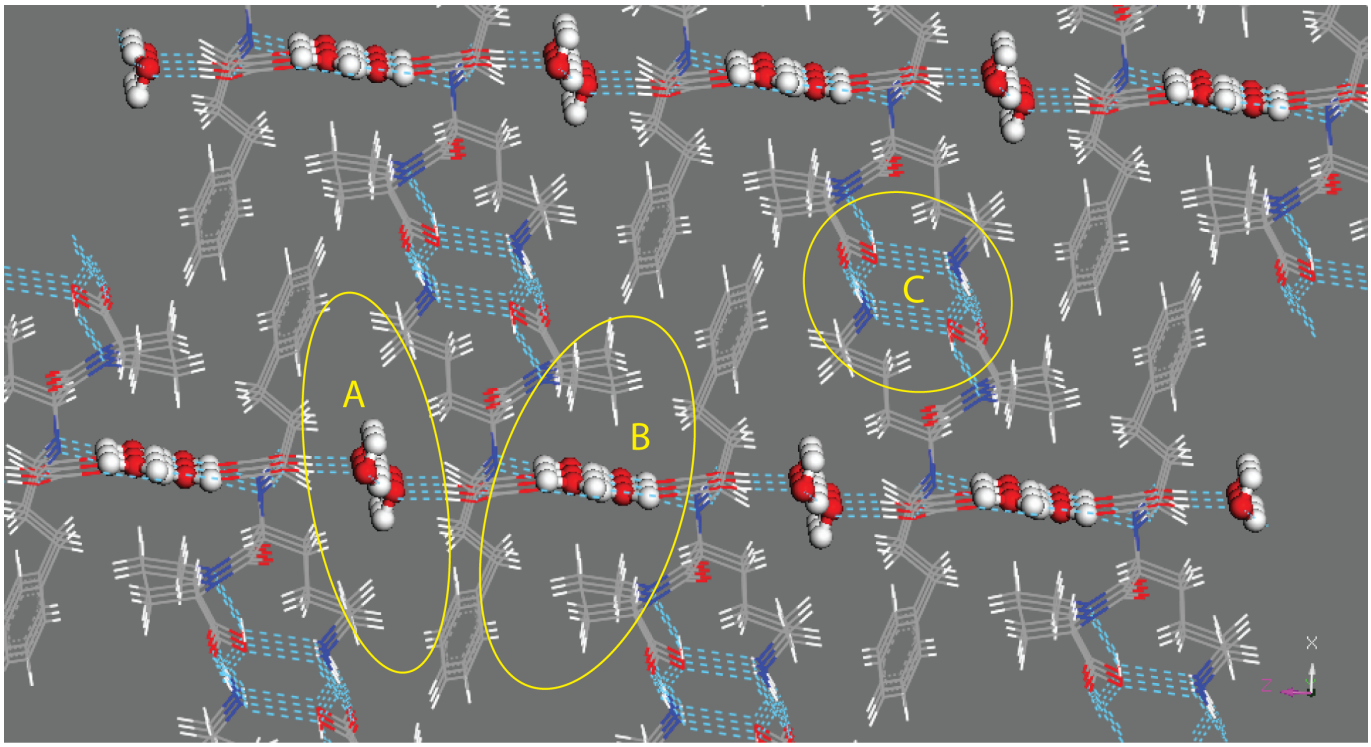

Fig. E2 *Long range ordering and the major crystal packing patterns identified in the* Lisi1$^{(0)}$ *crystal structure model: two distinct water channels created by columnar arrangements of Lisinopril molecules along the* b *crystallographic axis, with phenyl rings facing alkyl chains (**A**), and pyrrolidine rings (**B**); coupling of Lisinopril molecules along the* a *crystallographic axis through the $N1H_2$ amino and C21-OOH carboxyl groups (**C**). Similar patterns have been found in the* LisiRef$^{(0)}$ *and* Lisi2$^{(0)}$ *models, and therefore no longer shown. Differences occur with respect to the formed hydrogen bonding networks (blue dashed lines), and specific water-water and water-Lisinopril short contacts within the two channels (see details below).*

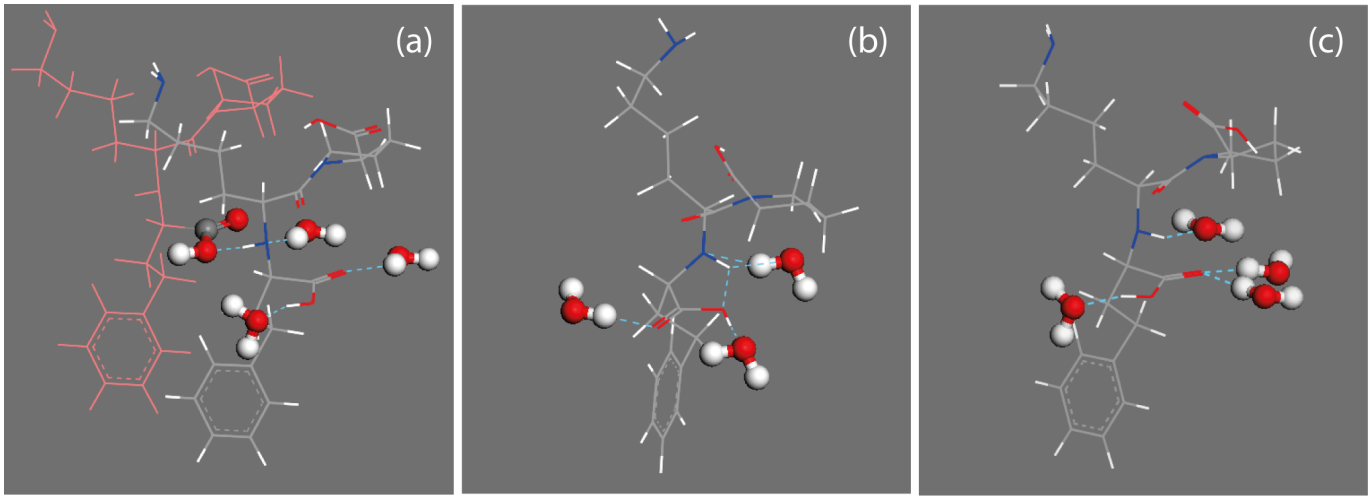

Fig. E3 *Hydrogen bonding patterns of a Lisinopril molecule in the median plane defined by the two water chains (*A *and* B *in Fig. E2) in the crystal structure models:* (a) LisiRef$^{(0)}$, (b) Lisi1$^{(0)}$, and (c) Lisi2$^{(0)}$. *The formation of a specific arrangement depends on the C10-OOH conformation and the value of the C16-C11-N2-H torsion angle of the Lisinopril molecule: the values of the associated geometric parameters are listed in* Table E3.

Table E3: Geometric parameters (D-A distance, and D-H-A angle) of the D-H…A hydrogen bonds in the crystal structure models shown in Fig. E3 depending on the specific values of the N2-C9-C10-O1 and C16-C11-N2-H torsion angles. Oxygen and hydrogen atoms of water molecules in the water channel *A(B)* are designated by $O_{B(A)}$ and $H_{B(A)}$. The intermolecular hydrogen bonds between adjacent Lisinopril molecules are represented in bold. All these intermolecular hydrogen bonds should be displayed twice in Fig. E3 – to not complicate the figure, this is omitted but must be assumed implicitly. Besides the hydrogen bonding networks of Lisinopril molecules shown in Fig. E3, the formed hydrogen bonds between water molecules are also given, but not shown in figure from the same reason. All these conventions will be considered in the rest of tables and figures below.

Model	< (N2-C9-C10-O1) / <(C16-C11-N2-H)	Hydrogen bonds (D-A distance / D-H-A angle)
LisiRef$^{(0)}$	158º / 179º	O1-H…O_A (2.65 Å; 15º); O_B-H_B…O2 (2.92 Å; 135º); O_B-H_B…N2 (2.71 Å; 162º); **N2-H…O1 (2.70 Å; 174º);** O_A-H_A…O_A (3.18 Å; 152^0);
Lisi1$^{(0)}$	-23º / -45º	O1-H…O_B (2.74 Å; 173º); O_A-H_A…O2 (2.63 Å; 176º); O_B-H_B…N2 (2.88 Å; 149º); N2-H…O_B (2.88 Å; 113º); N2-H…O1 (2.58 Å; 121^0); O_A-H_A…O_A (3.24 Å; 178^0);
Lisi2$^{(0)}$	156º / -77º	O1-H…O_A (2.75 Å; 153º); O_B-H_B…O2 (2.74 Å; 175º); O_B-H_B…O2 (2.83 Å; 152º); N2-H…O_B (2.88 Å; 154º);

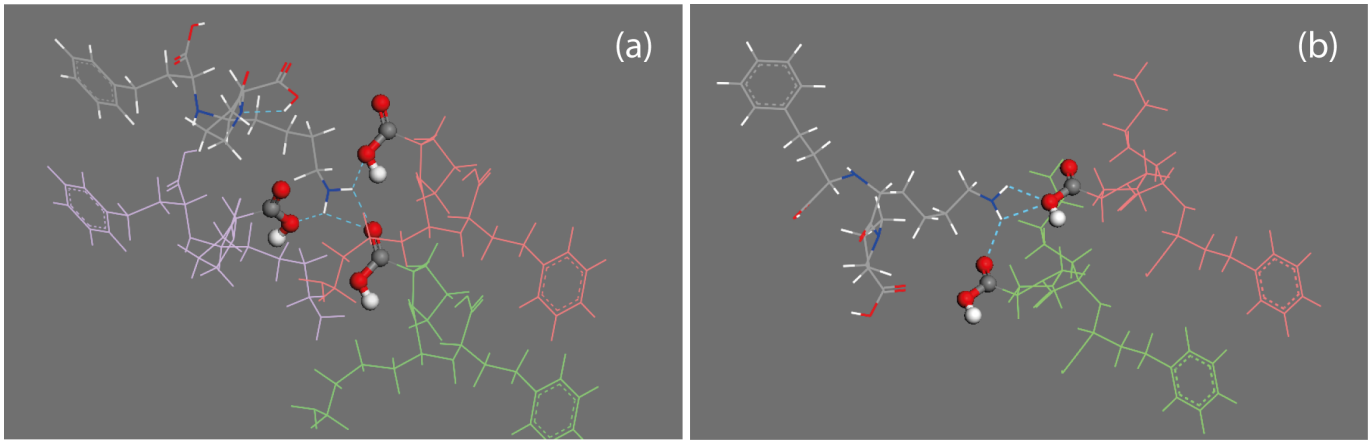

Fig. E4 *Hydrogen bonding patterns of a Lisinopril molecule around the N1 amine (*C *in Fig. E2) in the crystal structure models:* (a) LisiRef$^{(0)}$, and (b) Lisi2$^{(0)}$. *The pattern in* Lisi1$^{(0)}$ *was found identical to that in* LisiRef$^{(0)}$. *The formation of a specific arrangement depends on the C21-OOH conformation: the values of the associated geometric parameters are listed in* Table E4.

Table E4: Geometric parameters (D-A distance, and D-H-A angle) of the D-H…A hydrogen bonds formed around the N1 amine in investigated crystal structure models depending on the specific values of the N3-C17-C21-O4 torsion angle. Besides the intermolecular hydrogen bonds shown in Fig. E4, the O4-H…N3 intramolecular bond are also given.

Model	< (N3-C17-C21-O4)	Hydrogen bonds (D-A distance / D-H-A angle)
LisiRef$^{(0)}$	-5º	**N1-H…O4 (2.86 Å; 106º); N1-H…O4 (2.72 Å; 99º); N1-H…O5 (2.64 Å; 112º); N1-H…O5 (2.64 Å; 100º);** O4-H…N3 (2.55 Å; 127º);
Lisi1$^{(0)}$	-6º	**N2-H…O4 (2.82 Å; 104º); N2-H…O4 (2.79 Å; 110º); N2-H…O5 (2.68 Å; 115º); N2-H…O5 (2.68 Å; 97º);** O4-H…N3 (2.51 Å; 127^0);
Lisi2$^{(0)}$	174º	**N2-H…O4 (2.67 Å; 98º)**; **N2-H…O4 (2.67 Å; 109º)**; **N2-H…O5 (2.95 Å; 120º)**;

2. Analysis of the DFT computations

First-principle geometry optimization and NMR chemical-shift calculations were performed using the CASTEP and NMR CASTEP tools within the Accelrys Materials Studio® suite. CASTEP implements density functional theory (DFT) within a generalized gradient approximation and the plane wave pseudo-potential approach. All geometry optimizations and NMR chemical shift calculations used the PBE exchange-correlation functional, with ultrasoft pseudopotentials and a basis set cut-off energy of 810 eV. The geometry of the XRPD crystal structure solutions has been optimized (with the unit cell parameters fixed at their diffraction derived values) in two different ways: (i) first, only the positions of hydrogen atoms (the heavy atoms being fixed at their diffraction derived values) were optimized followed by optimization of the all atoms positions; (ii) direct optimization of the all atoms positions (including H atoms) of the XRPD crystal structure solutions. Forces, energies and displacements were converged better than 0.01 eV/Å, 0.000005 eV, and0.0005 Å, respectively. NMR chemical shift calculations (carried out on the structures following geometry optimisation) employed the GIPAW method to determine the shielding tensor for each nucleus in the crystal structure. The calculations used a plane wave basis set with a maximum cut-off energy of 810 eV, ultrasoft pseudopotentials generated on the fly, and integrals taken over the Brillouin zone by using a Monkhorst-Pack grid of minimum sample spacing 0.04 x 2π $Å^{-1}$.

Table E5: Comparative analysis of the *LisiRef*$^{(1)}$, *Lisi1*$^{(1)}$, and *Lisi2*$^{(1)}$, i.e., the previous $^{(0)}$ type crystal structure models with DFT geometry optimization of the all atoms positions, in terms of: energy variation ΔE relative to the lowest energy structure (*Lisi1*$^{(1)}$); RMSD of the Lisinopril molecular structure relative to the molecule in the *Lisi1*$^{(1)}$ (only the heavy atom positions are considered and no distinction between single and double bonded oxygen atoms in the carboxyl groups is made); C10-OOH / C21-OOH carboxyl groups conformations; ΔE` energy variation of the type $^{(1)}$ models relative to the energy in their type $^{(0)}$ counterparts; RMSD` - the RMSD between Lisinopril molecular structures in type $^{(1)}$ and $^{(0)}$ models (with respect to only the heavy atom positions); O-O distances and O-O-O angles between consecutive oxygen atoms in the *A* and *B* water chains.

Model	ΔE [kcal/mol]	Lisinopril RMSD [Å]	Carboxyls conformations C10-OOH / C21-OOH	ΔE` [kcal/mol]	Lisinopril RMSD` [Å]	O-O [Å] / O-O-O [^{0}]	
						water chain *A*	water chain *B*
LisiRef$^{(1)}$	46.4	0.035	a / -	-114.8	0.034	3.10 / 145	3.18 / 136
Lisi1$^{(1)}$	0	0	- / -	-129.9	0.017	3.09 / 146	3.31 / 126
Lisi2$^{(1)}$	103.5	0.146	a / a	-69.5	0.143	3.29 / 128	3.38 / 122

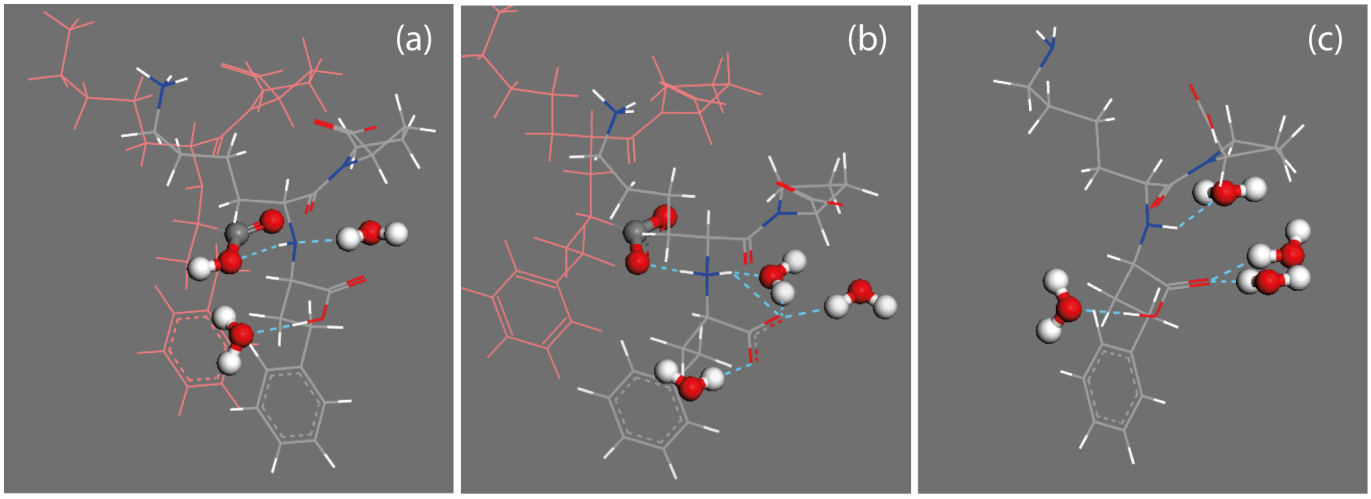

Fig. E5 *Hydrogen bonding patterns of a Lisinopril molecule in the median plane defined by the two water chains (*A *and* B *in Fig. E2) in the crystal structure models:* (a) LisiRef$^{(1)}$, (b) Lisi1$^{(1)}$, and (c) Lisi2$^{(1)}$. *The formation of a specific arrangement depends on the C10-OOH conformation and the value of the C16-C11-N2-H torsion angle of the Lisinopril molecule: the values of the associated geometric parameters are listed in* Table E6.

Table E6: Geometric parameters (D-A distance, and D-H-A angle) of the D-H…A hydrogen bonds in the crystal structure models shown in Fig. E5 depending on the specific values of the N2-C9-C10-O1(O′) and C16-C11-N2-H torsion angles – the O1-H proton transfer makes O1 and O2 indistinguishable in the *Lisi1*$^{(1)}$ model, and therefore they are both designated by O′.

Model	< (N2-C9-C10-O1) / <(C16-C11-N2-H)	Hydrogen bonds (D-A distance / D-H-A angle)
LisiRef$^{(1)}$	163° / -171°	O1-H…O_A (2.72 Å; 172°); O_B-H_B…N2 (2.89 Å; 163°); **N2-H…O1 (3.09 Å; 159°);** O_A-H_A…O_A (3.10 Å; 176°); O_B-H_B…O_B (3.18 Å; 132°);
Lisi1$^{(1)}$	-20° / -65°	O_A-H_A…O′ (2.75 Å; 176°); O_B-H_B…O′ (2.78 Å; 157°); O_B-H_B…O′ (2.72 Å; 155°); **N2-H…O′ (2.71 Å; 175°)**; N2-H…O′ (2.79 Å; 103°); N2-H…O_B (2.95 Å; 168°); O_A-H_A…O_A (3.09 Å; 175°);
Lisi2$^{(1)}$	164° / -81°	O1-H…O_A (2.76 Å; 172°); O_B-H_B…O2 (2.81 Å; 173°); O_B-H_B…O2 (2.86 Å; 148°); N2-H…O_B (3.01 Å; 143°); O_A-H_A…O_A (3.29 Å; 152°);

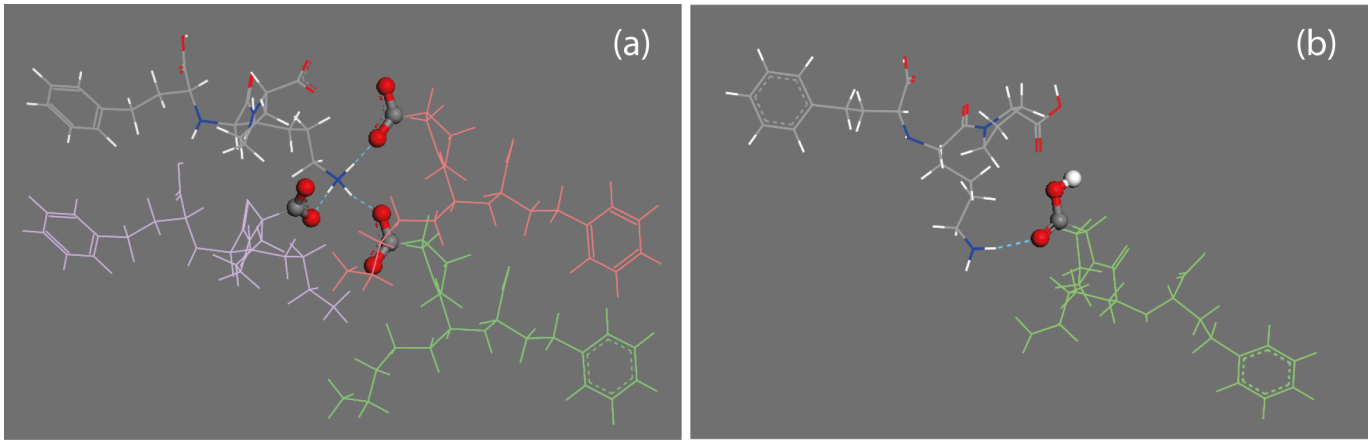

Fig. E6 *Hydrogen bonding patterns of a Lisinopril molecule around the N1 amine* (C *in Fig. E2*) *in the crystal structure models:* (a) LisiRef[(1)], and (b) Lisi2[(1)]. *The pattern in* Lisi1[(1)] *was found identical to that in* LisiRef[(1)]. *The formation of a specific arrangement depends on the C21-OOH conformation: the values of the associated geometric parameters are listed in* Table E7.

Table E7: Geometric parameters (D-A distance, and D-H-A angle) of the D-H…A hydrogen bonds formed around the N1 amine in the type [(1)] crystal structure models, depending on the specific values of the N3-C17-C21-O4(O″) torsion angle – the O4-H proton transfer makes O4 and O5 indistinguishable in the *LisiRef*[(1)] and *Lisi1*[(1)] models, and therefore they are both designated by O″.

Model	< (N3-C17-C21-O´) < (N3-C17-C21-O4)	Hydrogen bonds (D-A distance / D-H-A angle)
LisiRef[(1)]	-8º	**N1-H…O″ (2.71 Å; 163º); N1-H…O″ (2.75 Å; 172º); N1-H…O″ (2.76 Å; 172º);**
Lisi1[(1)]	-13º	**N1-H…O″ (2.77 Å; 172º); N1-H…O″ (2.75 Å; 163º); N1-H…O″ (2.77 Å; 173º);**
Lisi2[(1)]	160º	**N2-H…O5 (3.14 Å; 166º);**

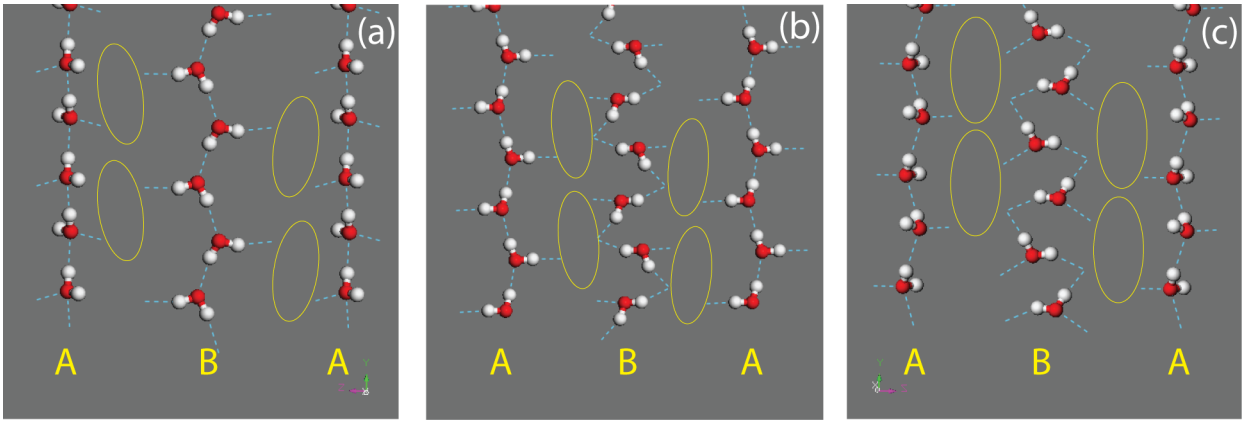

Fig. E7 *Water chains topology inside the* A *and* B *channels defined by the columnar arrangement of the Lisinopril molecules (sketched by yellow ellipses) and the associated hydrogen bonding networks in the crystal structure models:* (a) LisiRef[(1)], (b) Lisi1[(1)], and (c) Lisi2[(1)]. *The values of the corresponding geometric parameters are listed in* Table E5.

3. Analysis of the ss-NMR data

Solid-state ^{13}C, ^{15}N, and ^{1}H NMR spectra of Lisinopril dihydrate were recorded at 125.73, 50.66 and 499.98 MHz Larmor frequencies with a Bruker AVANCE III 500 MHz spectrometer operating at room temperature. Standard RAMP $^{13}C/^{15}N$ CP-MAS spectra were acquired at 15/7 kHz kHz spinning frequencies, 2/4 ms contact times, and proton decoupling under TPPM, by averaging 3000/20000 transients with a recycle delay of 3 s. ^{1}H ss-NMR spectra were acquired under both, free evolution at ultra-fast MAS (65 kHz), and homonuclear decoupling at 13.84 kHz spinning frequency. For the latter, the windowed eDUMBO-1_{22} sequence was used, with parameters first optimized on Glycine for best decoupling performances. A ^{13}C-^{1}H HETCOR 2D NMR spectrum was recorded by taking 92 points in the indirect time-domain under eDUMBO-1_{22} homonuclear decoupling and the States-TPPI scheme for phase sensitive detection. The distinct FIDs were acquired by averaging 512 transients with a recycle delay of 3 s. Mixing was achieved by short (85 μs) CP-MAS contact pulses of constant amplitudes: 40 and 55 kHz on the ^{13}C and ^{1}H channel. ^{13}C Cross-Polarization Polarization Inversion (CPPI) experiments at 15 kHz sample spinning were performed separately for CH_2 and aliphatic CH resonances, using also constant amplitudes CP. Prior to this, the direct CP contact times were optimized on Glycine and L-Alanine for maximum polarization transfer in CH_2 (75 μs), and CH groups (85 μs), respectively. For comparison, CPPI spectra were collected also on Glycine and L-Alanine. For CPPI data analysis, numerical simulations were performed with the SPINEVOLUTION program on representative 10-spin systems (one central ^{13}C, and the closest 9 protons), with atomic coordinates taken from the *Lisi1*[(1)] crystal structure solution, in the case of Lisinopril dihydrate. The recorded ^{13}C, ^{1}H, and ^{15}N NMR spectra are calibrated relative to the CH_3 line in TMS (tetramethylsilane), and the $^{15}NO_2$ line in nitromethane, through an indirect procedure which uses adamantane (1.8 ppm for ^{1}H; 38.5 ppm for ^{13}C) and Glycine (-347.6 ppm for ^{15}N) as external references.

^{15}N CP-MAS data:

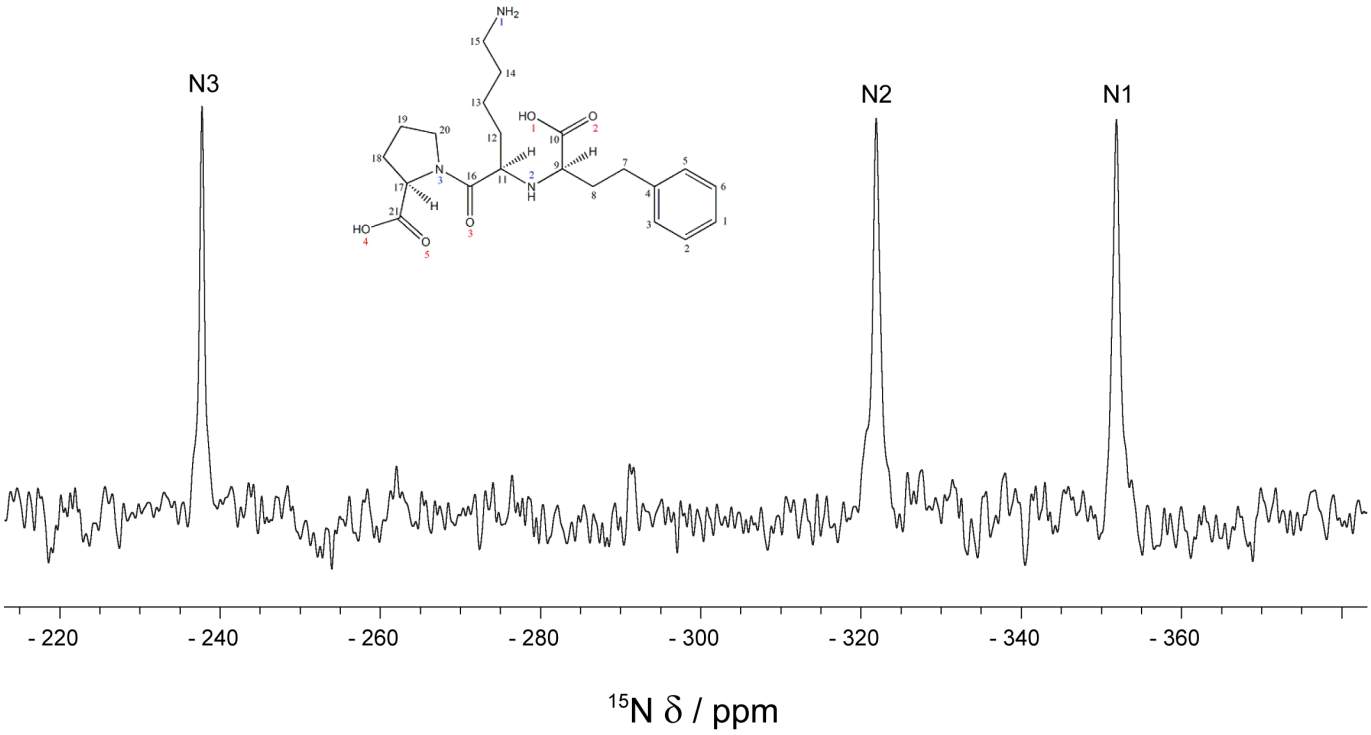

Fig. E8 *^{15}N CP-MAS spectrum of Lisinopril dihydrate. Spectral assignment was done by comparing the experimental chemical shifts with the results of the DFT computations, as described below in* Table E8.

Table E8: Experimental, $^{15}\delta_{exp}$, *vs* computed, $^{15}\delta_{calc}$, ^{15}N chemical shifts on the three crystal structure models. The theoretical chemical shift values were determined from the computed chemical shielding, $^{15}\sigma_{calc}$, through $^{15}\delta_{calc} = {}^{15}\sigma_{ref} - {}^{15}\sigma_{calc}$, with $^{15}\sigma_{ref}$ = -154 ppm extracted from previous studies [A.C. Uldry *et al*, *J. Am. Chem. Soc* **130** (2008) 945].

N site	$^{15}\delta_{exp}$ / ppm	$^{15}\delta_{calc}$ / ppm		
		***LisiRef*$^{(1)}$**	***Lisi1*$^{(1)}$**	***Lisi2*$^{(1)}$**
N1	-351.9	-351.1	-351.6	-325.5
N2	-321.9	-335.7	-321.2	-336.6
N3	-237.8	-227.6	-224.6	-243.5

1D ^{1}H NMR data:

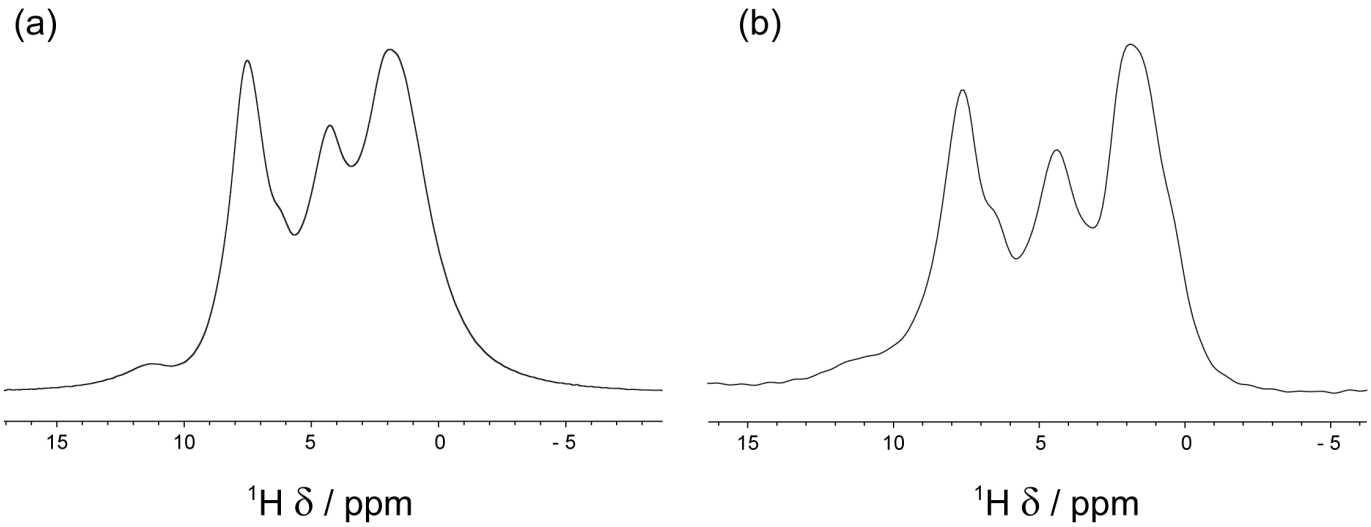

Fig. E9: *^{1}H ss-NMR spectra of Lisinopril dihydrate recorded under:* (a) *ultra-fast MAS at 65 kHz;* (b) *homonuclear decoupling by windowed eDUMBO-1$_{22}$ sequence at 13.84 kHz spinning frequency. Spectral resolution is fairly similar in the two cases: only partially resolved resonances could be obtained, which are peaked around 1.9 ppm, 4.3 ppm, 6.2 ppm, 7.5 ppm, and 11.3 ppm.*

^{13}C CP-MAS data:

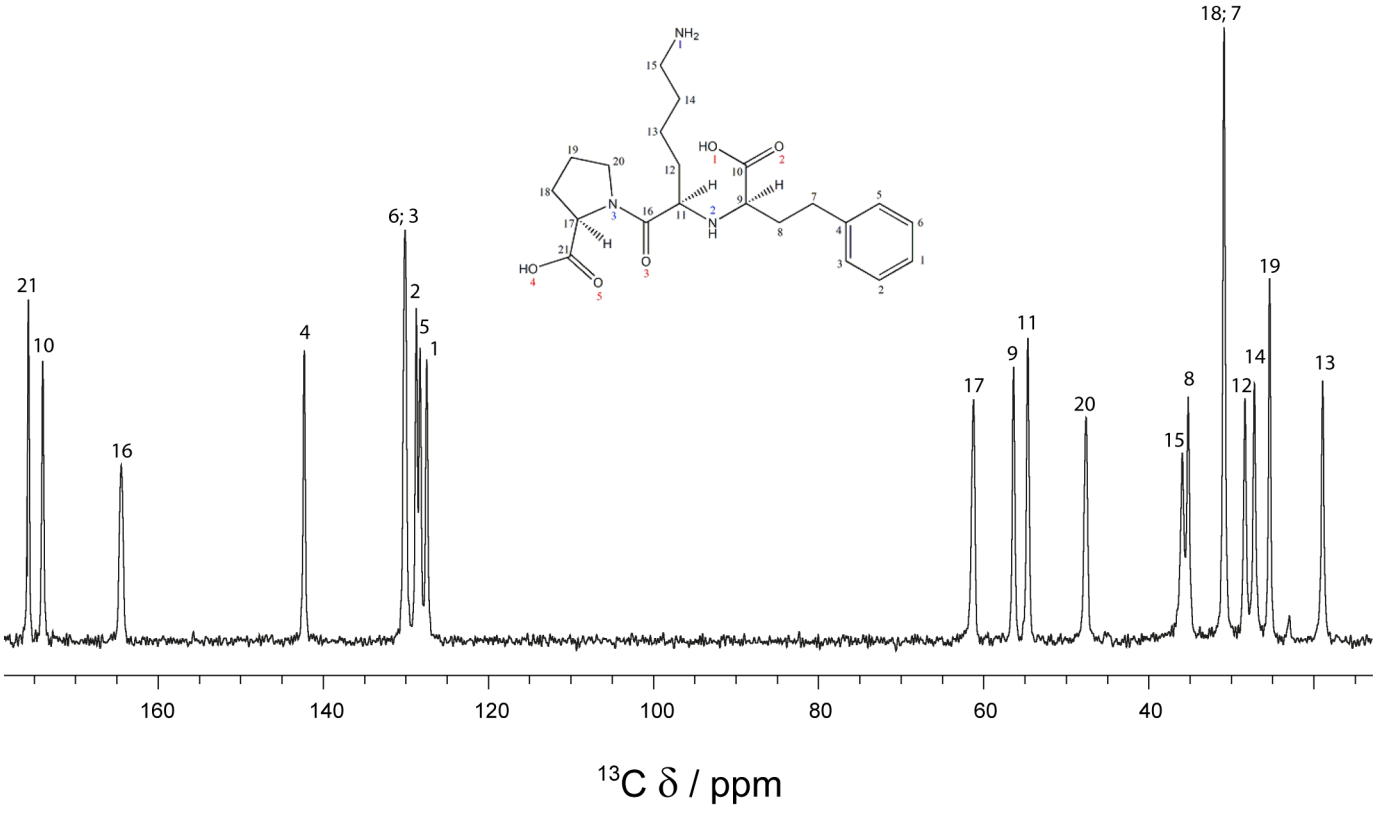

Fig. E10 *^{13}C CP-MAS spectrum of Lisinopril dihydrate. Spectral assignment was done by a mixed approach, which combines the results of the DFT computations* (Tab. E9) *with specific information extracted from a short mixing-time ^{1}H-^{13}C HETCOR spectrum* (Fig. E11), *and a systematic experimental and theoretical study by Cross-Polarization Polarization-Inversion (CPPI)* – Fig. E12 *and* Tab. E10. *The assignment procedure is summarized in* Table E11.

Table E9: Experimental, $^{13}\delta_{exp}$, *vs* computed, $^{13}\delta_{calc}$, ^{13}C chemical shifts on the *Lisi1*[1] and *LisiRef*[1] crystal structure models. The theoretical chemical shift values were determined from the computed chemical shielding, $^{13}\sigma_{calc}$, through $^{13}\delta_{calc} = {}^{13}\sigma_{ref} - {}^{13}\sigma_{calc}$, with $^{13}\sigma_{ref}$ extracted from linear fits of $^{13}\delta_{exp}$ *vs* $^{13}\delta_{calc}$, performed separately for the CH_2, aliphatic CH, aromatic CH, and carboxyl / carbonyl carbons. The C sites for which unambiguous assignment of the corresponding ^{13}C CP-MAS lines could be done are marked in red. The largest deviations between computed and measured chemical shifts, $^{13}\Delta = {}^{13}\delta_{calc} - {}^{13}\delta_{exp}$, are obtained for some alkyl, aromatic CH, and the C10 carboxyl resonances in *LisiRef*[1]. In the all other cases, the $^{13}\Delta$ values fall within typical ranges reported for good quality structural models. The RMSD values, given in the last line of the tables, are calculated for the all carbon sites.

Lisi1[1]

C site	$^{13}\sigma_{calc}$ / ppm	$^{13}\delta_{calc}$ / ppm	$^{13}\delta_{exp}$ / ppm	$^{13}\Delta$ / ppm
CH_2 group; $^{13}\sigma_{ref}$ = 171.3 ppm				
C13	153.9	17.4	18.9	-1.5
C19	146.6	24.7	25.3	-0.6
C14	145.3	26.0	27.2	-1.2
C12	143.9	27.4	28.3	-0.9
C7	139.8	31.5	30.9	0.6
C18	139.8	31.5	30.9	0.6
C15	135.6	35.7	35.2	0.5
C8	135.0	36.3	35.9	0.4
C20	121.5	49.9	47.6	2.3
Aliphatic CH; $^{13}\sigma_{ref}$ = 169.4 ppm				
C11	115.4	54.0	54.6	-0.6
C9	112.7	56.7	56.4	0.3
C17	107.9	61.5	61.2	0.3
Aromatic CH; $^{13}\sigma_{ref}$ = 167.7 ppm				
C1	40.1	127.6	127.4	0.2
C5	40.0	127.7	128.2	-0.5
C2	39.9	127.8	128.7	-0.9
C6	38.1	129.6	130.1	-0.5
C3	36.6	131.0	130.1	0.9
C4	24.8	142.9	142.3	0.6
Carboxyl / Carbonyl; $^{13}\sigma_{ref}$ = 167.8 ppm				
C16	4.6	163.2	164.4	-1.2
C10	-6.5	174.3	173.9	0.4
C21	-8.8	176.6	175.7	0.9
RMSD				**0.89**

LisiRef[1]

C site	$^{13}\sigma_{calc}$ / ppm	$^{13}\delta_{calc}$ / ppm	$^{13}\delta_{exp}$ / ppm	$^{13}\Delta$ / ppm
CH_2 group; $^{13}\sigma_{ref}$ = 170.0 ppm				
C13	154.3	15.7	18.9	3.2
C19	146.6	23.4	25.3	-1.9
C14	143.1	26.9	27.2	-0.3
C7	140.5	29.5	28.3	1.2
C18	138.8	31.2	30.9	0.3
C15	137.1	32.9	30.9	2.0
C12	136.6	33.4	35.2	-1.8
C8	131.5	38.5	35.9	2.6
C20	121.4	48.6	47.6	1.0
Aliphatic CH; $^{13}\sigma_{ref}$ = 170.4 ppm				
C11	115.4	55.0	54.6	0.4
C9	115.0	55.4	56.4	-1.0
C17	108.7	61.7	61.2	0.5
Aromatic CH; $^{13}\sigma_{ref}$ = 167.4 ppm				
C5	41.0	126.4	127.4	-1.0
C1	40.4	127.1	128.2	-1.1
C2	38.5	128.9	128.7	0.2
C6	37.9	129.5	130.1	-0.6
C3	37.3	130.1	130.1	0.0
C4	22.6	144.8	142.3	2.5
Carboxyl / Carbonyl; $^{13}\sigma_{ref}$ = 166.6 ppm				
C16	1.3	165.3	164.4	0.9
C10	-5.2	171.8	173.9	-2.1
C21	-10.4	177.0	175.7	1.3
RMSD				**1.51**

^{1}H-^{13}C HETCOR data:

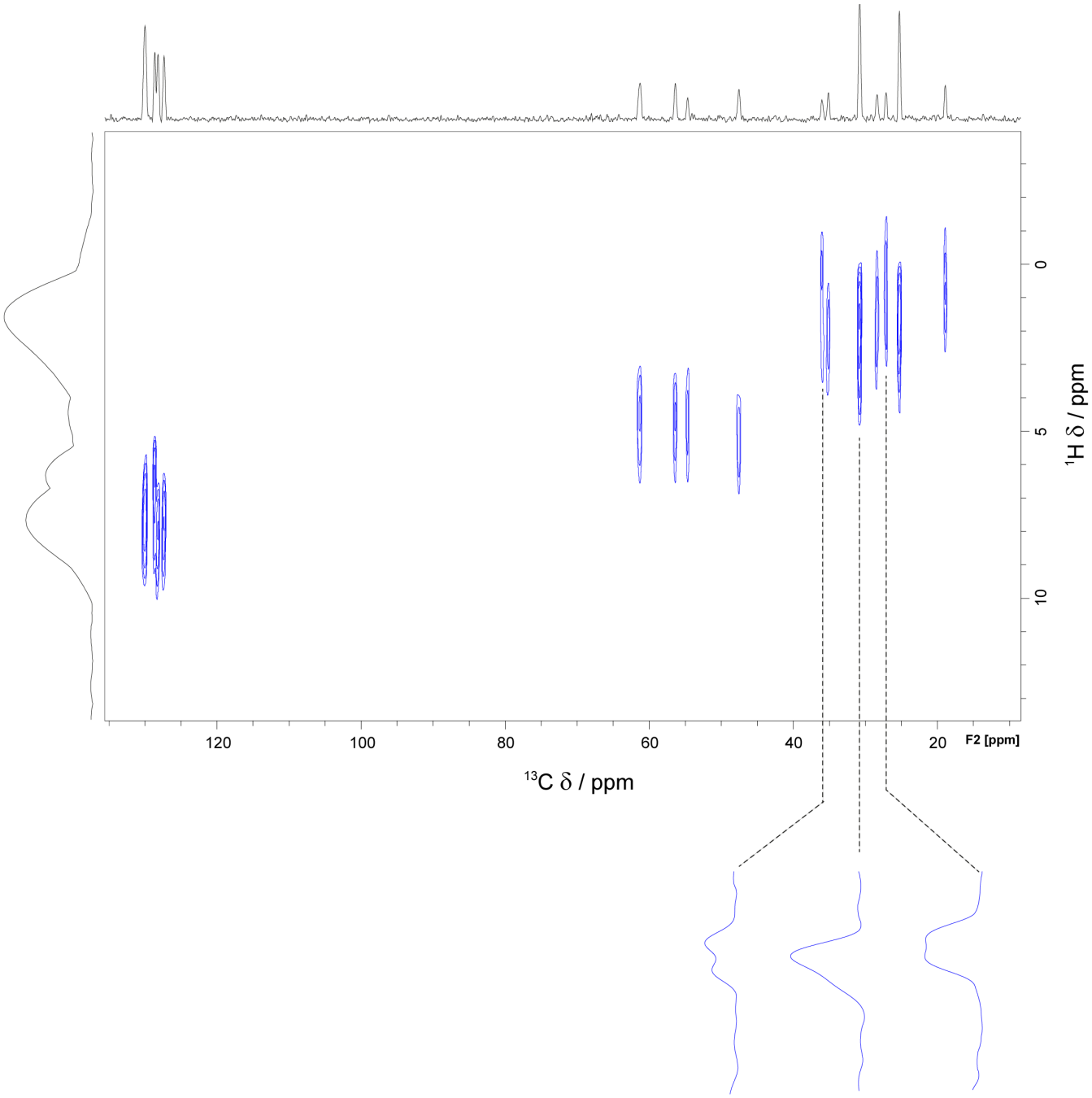

Fig. E11 *^{1}H- ^{13}C HETCOR spectrum of Lisinopril dihydrate. The correlation peaks corresponding to the 27.2, 30.9 and 35.9* ppm *^{13}C resonances display partially resolved lines along ^{1}H dimension (the corresponding slices are shown). They are associated with CH_2 groups for which one of the protons is in the close neighborhood of a phenyl ring and experiences ^{1}H line shift due to ring current effects. Considering the crystal packing obtained in the all investigated Lisinopril dihydrate models, these methylen groups corresponds to the C14, C7 and C15 carbon sites. From the projection along ^{13}C dimension, it is to be noted also the much larger amplitude of the lines at 25.3 and 30.9* ppm *compared with the rest of the alkyl chain ^{13}C resonances. This is due to a significant line narrowing of the corresponding peaks along ^{1}H dimension, which is assumed of having a motional origin. The assumption was confirmed by analyzing the ^{13}C→ ^{1}H polarization transfer dynamics in suitably calibrated Cross-Polarization Polarization-Inversion (CPPI) experiments (see below in* Fig. E12, *and* Tab. E10*).*

^{13}C CPPI data:

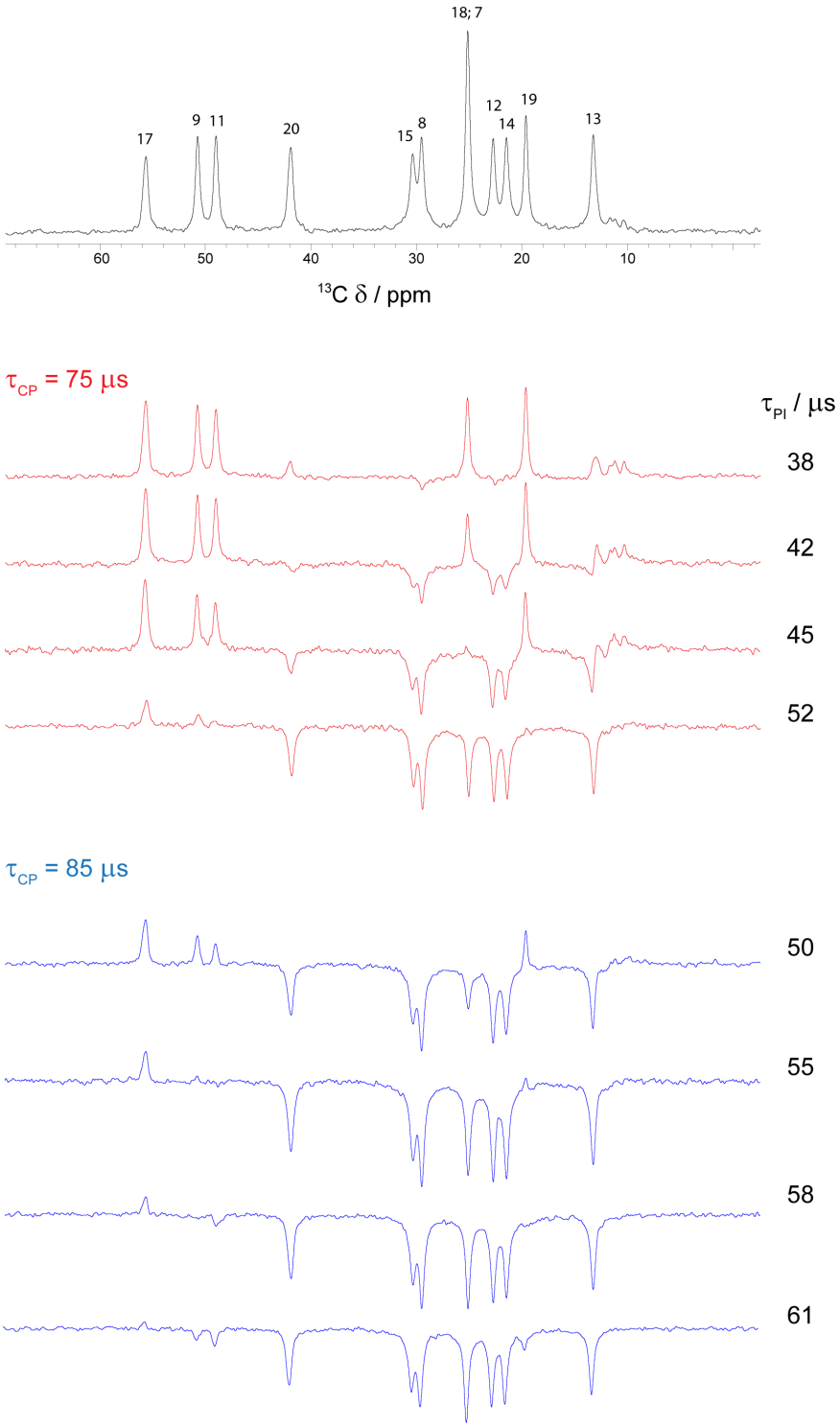

Fig. E12 *Expansion of the aliphatic region of the ^{13}C CP-MAS spectrum of Lisinopril dihydrate (top figure). Selected slices from the CPPI data sets recorded with values of the direct CP time τ_{CP} adjusted for maximum polarization transfer inside CH_2 (red) and aliphatic CH (blue) moieties. In the two separate CPPI experiments, the values of the polarization inversion time τ_{PI} was varied in the range 35-55 µs for CH_2, and 50-65 µs for CH, such as to cover the inversion of the all corresponding NMR resonances. The quantitative analysis of the CPPI results is summarized in* Table E10 *below.*

Table E10: Representative results of the ^{13}C CPPI data analysis. Two CPPI data sets were recorded with τ_{CP} optimized first for maximum ^{1}H-> ^{13}C polarization transfer within CH (on L-Alanine model system: τ_{CP} = 85 μs) and CH_2 (on Glycine model system: τ_{CP} = 75 μs). The Polarization-Inversion ^{13}C -> ^{1}H duration, τ_{PI}, was swept in the range 35 - 55 μs and 50 - 65 such as to cover the inversion of the all CH_2 and CH ^{13}C resonance lines in Lisinopril dihydrate. The corresponding values for the signal cancellation time, $\tau_{PI,exp}$, are given in the second column of the table. In each case, the smallest $\tau_{PI,exp}$ value (36 μs for CH_2, and 55 μs for CH, respectively) was taken as reference for a quasi-rigid behavior. Large deviations $\Delta = \tau_{PI,exp} - \tau_{PI,reference}$ with respect to these minimum values are assumed to be caused by fast molecular motion associated with that particular site (the C-H dipolar coupling strength being reduced by a factor *S* compared with the dipolar coupling in rigid CH and CH_2 moieties). A series of numerical simulations performed on selected (^{13}C, *n* ^{1}H, with *n* = 1÷9) spin systems depicted from the crystal structure model *Lisi1*[(1)] have shown that up to 4 μs of the Δ values could come from differences in the proton environment of a given ^{13}C site, so that only the resonances marked in red were considered as being affected by molecular motion with certainty, and included in the study. The listed scaling factors *S* were calculated in each case based on simulations performed in simplified CH and CH_2 systems. Therefore, they should be considered only a semi-quantitative measure for the relative amplitudes of the molecular motion affecting different sites. For comparison, the polarization inversion time measured on the considered model systems, $\tau_{PI,model}$, are also given (on L-Alanine for CH, and on Glycine for CH_2, respectively).

$^{13}\delta_{exp}$ / ppm	$\tau_{PI,exp}$ / μs	$\tau_{PI,sim}$ / μs	Δ / μs	S
CH_2 group; $\tau_{CP,model}$ = 75 μs, $\tau_{PI,model}$ = 38 μs				
18.9	43	29÷32	7	0.86
25.3	52		16	0.69
27.2	38		2	
28.3	37		1	
30.9	46		10	0.79
30.9	-		-	-
35.2	36		0	-
35.9	38		2	-
47.5	41		5	0.89
Aliphatic CH; $\tau_{CP,model}$ = 85 μs, $\tau_{PI,model}$ = 60 μs				
54.6	55	50÷54	0	-
56.4	58		3	-
61.2	63		8	0.87

Table E11: Summary of the ^{13}C, and ^{1}H (partial) ss-NMR spectral assignment procedure used in the present work, which combines the results of DFT quantum chemical computations with specific information extracted from the analysis of the short mixing time ^{1}H-^{13}C HETCOR spectrum (Fig. E11), and the CPPI data (Fig. E12, and Tab. E10). In the case of the resonances for which the experimental data were employed, the unambiguous assignment was achieved by taking into account also the closest $^{13}\delta_{calc}$ values. For the other ^{13}C resonances, the assignment was finally considered from the best fit of $^{13}\delta_{exp}$ *vs* $^{13}\delta_{calc}$, which was obtained for the *Lisis1*[(1)] model (Tab. E12).

$^{13}\delta_{exp}$ / ppm	$^{1}\delta_{exp}$ / ppm	Assignment	Arguments
18.9	0.9	C13 / H13	$^{13}\delta_{calc}$
25.3	1.6	C19 / H19	puckering dynamics with the largest amplitude inside the pyrrolidine ring + the closest $^{13}\delta_{calc}$
27.2	0.2/1.6	C14 / H14	partial resolution of the H14 protons due to the phenyl ring-current effect + the closest $^{13}\delta_{calc}$
28.3	1.8	C12 / H12	the closest $^{13}\delta_{calc}$
30.9	1.5	C18 / H18	puckering dynamics with the second largest amplitude inside the pyrrolidine ring + the closest $^{13}\delta_{calc}$
30.9	?/3.8	C7 / H7	partial resolution of the H7 protons due to the phenyl ring-current effect + the closest $^{13}\delta_{calc}$: the low ppm ^{1}H H7 line could not be identified due to the superposition with the intense H18 line
35.2	2.0	C8 / H8	the closest $^{13}\delta_{calc}$
35.9	0.2/2.6	C15 / H15	partial resolution of the H15 protons due to the phenyl ring-current effect + the closest $^{13}\delta_{calc}$
47.5	5.2	C20 / H20	$^{13}\delta_{calc}$ + puckering dynamics of lower amplitude inside the pyrrolidine ring
54.6	4.5	C11 / H11	$^{13}\delta_{calc}$
56.4	4.6	C9 / H9	$^{13}\delta_{calc}$
61.2	4.4	C17 / H17	puckering dynamics of lower amplitude inside the pyrrolidine ring + the closest $^{13}\delta_{calc}$
127.4	7.8	C1 / H1	$^{13}\delta_{calc}$
128.2	7.9	C5 / H5	$^{13}\delta_{calc}$
128.6	6.3	C2 / H2	$^{13}\delta_{calc}$
130.1	7.6	C6 / H6	$^{13}\delta_{calc}$
130.1	7.6	C3 / H3	$^{13}\delta_{calc}$
142.3	-	C4	$^{13}\delta_{calc}$
164.4	-	C16	$^{13}\delta_{calc}$
173.9	-	C20	$^{13}\delta_{calc}$
175.7	-	C21	$^{13}\delta_{calc}$

Table E12: Experimental, $^{13}\delta_{exp}$, *vs* computed, $^{13}\delta_{calc}$, ^{13}C chemical shifts on the *Lisi1*[(1)] and *LisiRef*[(1)] crystal structure models, where $^{13}\delta_{exp}$ correspond now to the data listed in Table E11. The theoretical chemical shift values $^{13}\delta_{calc}$ were determined from the computed chemical shielding, $^{13}\sigma_{calc}$, as before. Being based on the correct spectral assignment, large values of absolute deviations between computed and measured chemical shifts, $^{13}\Delta = {}^{13}\delta_{calc} - {}^{13}\delta_{exp}$, (marked in red) can be directly correlated with corresponding deviations of local structural parameters with respect to the real crystal structure of Lisinopril dihydrate. In the case of *LisiRef*[(1)] model they mainly refer to the conformation of the alky chain and local features around the C10-OOH carboxyl, whereas in *Lisi1*[(1)] only the C20 site seems to be affected.

Lisi1[(1)]

C site	$^{13}\sigma_{calc}$ / ppm	$^{13}\delta_{calc}$ / ppm	$^{13}\delta_{exp}$ / ppm	$^{13}\Delta$ / ppm
CH_2 group; $^{13}\sigma_{ref}$ = 171.3 ppm				
C13	153.9	17.4	18.9	-1.5
C19	146.6	24.7	25.3	-0.6
C14	145.3	26.0	27.2	-1.2
C12	143.9	27.4	28.3	-0.9
C18	139.8	31.5	30.9	0.6
C7	139.8	31.5	30.9	0.6
C8	135.0	36.3	35.2	1.1
C15	135.6	35.7	35.9	-0.2
C20	121.5	49.9	47.6	2.3
Aliphatic CH; $^{13}\sigma_{ref}$ = 170.2 ppm				
C11	115.4	54.0	54.6	-0.6
C9	112.7	56.7	56.4	0.3
C17	107.9	61.5	61.2	0.3
Aromatic CH; $^{13}\sigma_{ref}$ = 167.7 ppm				
C1	40.1	127.6	127.4	0.2
C5	40.0	127.7	128.2	-0.5
C2	39.9	127.8	128.7	-0.9
C6	38.1	129.6	130.1	-0.5
C3	36.6	131.0	130.1	0.9
C4	24.8	142.9	142.3	0.6
Carboxyl / Carbonyl; $^{13}\sigma_{ref}$ = 165.6 ppm				
C16	4.6	163.2	164.4	-1.2
C10	-6.5	174.3	173.9	0.4
C21	-8.8	176.6	175.7	0.9
RMSD				**0.91**

LisiRef[(1)]

C site	$^{13}\sigma_{calc}$ / ppm	$^{13}\delta_{calc}$ / ppm	$^{13}\delta_{exp}$ / ppm	$^{13}\Delta$ / ppm
CH_2 group; $^{13}\sigma_{ref}$ = 170.0 ppm				
C13	154.3	15.7	18.9	3.2
C19	146.6	23.4	25.3	1.9
C14	143.1	26.9	27.2	0.3
C12	136.6	33.4	28.3	-5.1
C18	138.8	29.5	30.9	1.4
C7	140.5	31.2	30.9	-0.3
C8	131.5	38.5	35.2	-3.3
C15	137.1	32.9	35.9	3.0
C20	121.4	48.6	47.6	-1.0
Aliphatic CH; $^{13}\sigma_{ref}$ = 170.4 ppm				
C11	115.4	55.0	54.6	-0.4
C9	115.0	55.4	56.4	1.0
C17	108.7	61.7	61.2	-0.5
Aromatic CH; $^{13}\sigma_{ref}$ = 167.4 ppm				
C1	40.4	127.0	127.4	0.4
C5	41.0	126.4	128.2	1.8
C2	38.5	128.9	128.7	-0.2
C6	37.9	129.5	130.1	0.6
C3	37.3	130.1	130.1	0.0
C4	22.6	144.8	142.3	-2.5
Carboxyl / Carbonyl; $^{13}\sigma_{ref}$ = 166.6 ppm				
C16	1.3	165.3	164.4	-0.9
C10	-5.2	171.8	173.9	2.1
C21	-10.4	177.0	175.7	-1.3
RMSD				**1.97**

Table E13: Experimental, $^1\delta_{exp}$, *vs* computed, $^1\delta_{calc}$, ^{1}H chemical shifts on the *Lisi1*$^{(I)}$ and *LisiRef*$^{(I)}$ crystal structure models. The theoretical chemical shift values were determined from the computed chemical shielding, $^1\sigma_{calc}$, through $^1\delta_{calc} = {}^1\sigma_{ref} - {}^1\sigma_{calc}$, with $^1\sigma_{ref}$ = 31 ppm. Where partially resolved ^{1}H lines are obtained in the ^{1}H-^{13}C HETCOR spectrum (Fig. E11), the comparison is done with respect to $^1\delta_{calc}$ for each individual proton of the corresponding CH_2 group, whereas in the rest, averaged values are employed (all are marked in bold). The CH_2 resonances show a reasonably good agreement between measured and computed ^{1}H chemical shifts, except H19, H18 and H15, for which the $^1\Delta = {}^1\delta_{calc} - {}^1\delta_{exp}$ values range between 0.4 and 1.1 ppm: interestingly, these protons belong to methylene groups for which fast molecular motion was concluded based on the CPPI data (Tab. E10). The aliphatic CH's show good agreement between $^1\delta_{exp}$ and $^1\delta_{calc}$, but this is slightly worse for aromatic CH's. In the both cases, better results are obtained for the *Lisi1*$^{(I)}$ model. The limited spectral resolution even under ultra-fast MAS, or homonuclear decoupling, leaves only the partially resolved ^{1}H line at11.3 ppm that can be further discussed: in the *LisiRef*$^{(I)}$ model, it can be assigned to the O1-H hydroxyl involved in the O1-H…O_A with a water molecule in channel *A*, whereas in the *Lisi1*$^{(I)}$ it corresponds to the proton in the N2-H_2^+ group which is involved in a N2-H…O´ hydrogen bond. This result, however, does not necessarily mean that there is no C10-OO⊖ -> N2-H_2^+ proton transfer, because the 1.2 ppm deviation between $^1\delta_{calc}$ and $^1\delta_{exp}$ in *Lisi1*$^{(I)}$ could in principle be caused also by slight deviations of the computed N2-H… O´ hydrogen bond parameters with respect to their actual values in the real structure of Lisisnopril dihydrate.

Lisi1$^{(I)}$

H site	**$^1\delta_{calc}$ / ppm**		**$^1\delta_{exp}$ / ppm**	**$^1\Delta$ / ppm**
	Individual	Average		
CH_2 group				
H13a / H13b	0.8 / 0.6	**0.7**	0.7	0.0
H19a / H19b	1.9 / 3	**2.4**	1.6	0.8
H14a / H14b	**0.5 / 1.3**	-	0.2 / 1.5	0.3 / -0.2
H12a / H12b	1.7 / 1.9	**1.8**	1.7	0.1
H18a / H18b	1.6 / 2.4	**2.0**	1.6	0.4
H7a / H7b	**2.4 / 3.8**	-	? / 3.8	? / 0
H8a / H8b	2.2 / 2.5	**2.3**	2.1	0.2
H15a / H15b	**0.5 / 2.2**	-	0.2 / 2.6	0.3 / -0.4
H20a / H20b	4.5 / 5.7	**5.1**	5.2	-0.1
Aliphatic CH				
H11	4.3	-	4.5	-0.2
H9	4.8	-	4.6	0.2
H17	4.4	-	4.4	0.0
Aromatic CH				
H1	7.6	-	7.8	-0.2
H5	7.5	-	7.9	-0.4
H2	6.3	-	6.3	0
H6	7.2	-	7.6	-0.4
H3	7.2	-	7.6	-0.4
Amines / Hydroxyl / Water				
N1: Ha / Hb / Hc	8.2 / 7.1 / 9.5	-	-	-
N2: H	8.5 / **12.5**	-	11.3	1.2
O1: H	-	-	-	-
Water *A*: Ha / Hb	3.2 / 6.5	-	-	-
Water *B*: Ha / Hb	5.5 / 5.8	-	-	-

LisiRef$^{(I)}$

H site	**$^1\delta_{calc}$ / ppm**		**$^1\delta_{exp}$ / ppm**	**$^1\Delta$ / ppm**
	Individual	Average		
CH_2 group				
H13a / H13b	0.6 / 0.9	**0.7**	0.7	0
H19a / H19b	1.7 / 3.7	**2.7**	1.6	1.1
H14a / H14b	**0.1 / 1.7**	-	0.2 / 1.5	-0.1 / 0.2
H12a / H12b	1.1 / 1.7	**1.4**	1.7	-0.3
H18a / H18b	1.5 / 2.5	**2.0**	1.6	0.4
H7a / H7b	**2.5 / 3.8**	-	? / 3.8	? / 0
H8a / H8b	1.7 / 2.6	**2.1**	2.1	0
H15a / H15b	**0.5 / 2.4**	-	0.2 / 2.6	0.3 / -0.2
H20a / H20b	4.6 / 5.4	**5.0**	5.2	-0.2
Aliphatic CH				
H11	4.2	-	4.5	-0.3
H9	4.3	-	4.6	-0.3
H17	4.6	-	4.4	0.2
Aromatic CH				
H1	7.4	-	7.8	-0.4
H5	7.3	-	7.9	-0.6
H2	6.1	-	6.3	-0.2
H6	7.0	-	7.6	-0.6
H3	7.1	-	7.6	-0.5
Amines / Hydroxyl / Water				
N1: Ha / Hb / Hc	7.2 / 8.6 / 10.1	-	-	-
N2: H	4.0	-	-	-
O1: H	11.6	-	11.3	0.3
Water *A*: Ha / Hb	3.7 / 5.5	-	-	-
Water *B*: Ha / Hb	4.4 / 4.7	-	-	-